


Statistically averaged molecular dynamics simulations of hydrogen diffusion in magnesium and magnesium hydrides

C. D. Spataru,¹ T. W. Heo,² B. C. Wood,² V. Stavila,¹ S. Kang,² M. D. Allendorf,¹ and X. W. Zhou^{1,*}

¹Sandia National Laboratories, Livermore, California 94550, USA

²Lawrence Livermore National Laboratory, Livermore, California 94550, USA

 (Received 21 May 2020; revised 3 September 2020; accepted 15 September 2020; published 5 October 2020)

Magnesium has a different crystal structure from its dihydride with hydrogenation leading to a phase transition from the hexagonal closely packed Mg into a tetragonal α -MgH₂ rutile type structure. Such materials exhibit complex hydrogen uptake and release kinetics because hydrogen diffusivities significantly change when the crystal structure changes. To provide a foundational understanding of (de)hydrogenation kinetics that is applicable to all stages of the reaction, we performed statistically averaged molecular dynamics simulations to derive hydrogen diffusivities as a function of temperature and hydrogen content for both magnesium and magnesium hydride. Our studies confirm that hydrogen diffusivities in magnesium hydride are much lower than in magnesium, in agreement with experimental data. Additionally, we observe that in either magnesium or magnesium hydride, higher hydrogen compositions result in reduced diffusivities. The latter was not revealed by prior experiments, which were conducted at fixed hydrogen composition. Finally, we discover a non-Arrhenius behavior in magnesium hydride. The physical origin of this behavior is also discussed.

DOI: [10.1103/PhysRevMaterials.4.105401](https://doi.org/10.1103/PhysRevMaterials.4.105401)

I. INTRODUCTION

Metal hydrides are attractive for vehicular hydrogen storage because hydrogen can be stored at noncryogenic temperatures and at much lower pressures than the 700 bars currently used in compressed gas tanks [1]. One major challenge is that the kinetics of hydrogen uptake and release for many metal hydrides considered for storage applications is not fast enough to meet the technical targets defined by the U.S. DOE (see, for example, the Hydrogen Tech Team Roadmap [2]). Various mechanisms postulated for hydriding and dehydriding reactions are often rate limited by hydrogen diffusion. Unfortunately, hydrogen diffusivity is not a constant and changes continuously as the hydrogen composition varies during reaction. This change can be abrupt when a phase transformation between a metal and the corresponding hydride occurs. As a result, the evolution of hydrogen diffusivity during (de)hydrogenation cannot be easily quantified from data obtained in prior experimental studies [3–13].

Magnesium hydride is an example of a so-called “transformational” solid-state hydrogen storage material because magnesium and magnesium hydride have different crystal structures: hexagonal closely packed (hcp) structure for Mg and tetragonal rutile structure for α -MgH₂. This contrasts with diffusional systems such as PdH_x, for which palladium and palladium hydride have the same face-centered cubic (fcc) crystal structure. Although its intrinsic hydrogen storage performance is insufficient for light-duty vehicular applications, MgH_x is an important model system for understanding key mechanisms of coupled chemical and transport processes,

which are generally applicable to more complex, higher-capacity metal hydrides such as Mg(BH₄)₂ [14]. In the case of PdH_x, extensive experiments have been performed to measure hydrogen diffusivities [8–13]. Compared to PdH_x, diffusivity data for MgH_x are relatively sparse [3–7]. In Table I we compile the available literature experimental data for the activation energy Q and preexponential factor D_0 for Mg and MgH_x systems. The literature activation energy values obtained from density-functional-theory (DFT) calculations [15–19] are also included. Typically, literature experiments were performed at a fixed hydrogen composition, either near Mg or near MgH₂. It is therefore unclear how hydrogen diffusion varies at various stages of magnesium (de)hydrogenation. In addition, the experimental parameters listed in Table I correspond to averaged bulk values, which masks the orientation dependence of diffusivity arising from crystallographic anisotropy. In particular, for the equilibrium hcp phase of Mg and tetragonal rutile phase of MgH₂, the diffusivities parallel and normal to the basal plane are different. Due to this anisotropy, experimental diffusivity is sensitive to grain structure (e.g., single crystal vs polycrystal), grain morphology, and sample texture, as well as potentially the measurement orientation. These factors add difficulty in rationalizing the discrepancies among the reported experimental data from different groups. Literature DFT values of diffusion energy barriers in MgH₂ are even more diverse. This is because the DFT values depend on hydrogen charge state, diffusion paths, and diffusion species (hydrogen vacancy or hydrogen interstitial). Here we only discuss hydrogen vacancies because hydrogen storage materials usually operate below the stoichiometric composition.

Statistically averaged molecular dynamics (MD) simulation [20–23] can be used to rapidly explore hydrogen diffusion across a wide range of hydrogen composition for

*Corresponding author: xzhou@sandia.gov

TABLE I. Measured activation energy barrier Q (in eV) and preexponential factor D_0 (in $\text{\AA}^2/\text{ps}$) as a function of phase and temperature T (in K).

| Experimental | | | | |
|---|------------------|--|------|-----------------------|
| Authors | Phase | T | Q | D_0 |
| Nishimura <i>et al.</i> [3] | Mg | 473–493 | 0.25 | 1.54×10^2 |
| Renner and Grabke [4] | Mg | 700–800 | 0.41 | 3.80×10^2 |
| Cermak and Kral [5] | MgH ₂ | 578–698 | 0.99 | 1.36×10^4 |
| Yao <i>et al.</i> [6] | MgH ₂ | 373–573 | 1.12 | 1.50×10^{-1} |
| Fernandez and Sanchez [7] | MgH ₂ | 570–670 | 1.04 | – |
| DFT at 0 K ^a | | | | |
| Authors | Phase | Q | | |
| van de Walle and co-workers (Ismer <i>et al.</i> [15], Sander <i>et al.</i> [16], Park <i>et al.</i> [17]) | MgH ₂ | 0.38 (+1 charge) 0.63 (–1 charge) | | |
| Sander <i>et al.</i> [16] | MgH ₂ | 0.37–0.38 (+1 charge) 1.14–1.72 (–1 charge) | | |
| German and Gebauer [19] | MgH ₂ | 0.79–1.10 (0 charge) | | |

^aValues listed in the original references vary widely depending on H charge state, diffusion path, system stoichiometry, and Fermi level.

both hydrogenated and dehydrogenated phases, as has been demonstrated successfully for PdH_{*x*} [20]. However, less simulations have been done on hydrogen diffusion in transformational systems. Since many promising metal hydrides under consideration for hydrogen storage involve both diffusional and phase-transformational processes (e.g., borohydrides and amides), a foundational understanding of hydrogen diffusion in transformational hydrides is essential for identifying rate limitations and developing improvement strategies.

Here we use MgH_{*x*} as a prototypical transformational metal hydride to achieve three major objectives: (i) apply statistically averaged MD methods [20–23] to calculate hydrogen diffusivities as a function temperature and composition for both hcp Mg and rutile MgH₂; (ii) fit the MD diffusivities to an analytical expression to facilitate the development of large-scale kinetics models describing the (de)hydrogenation processes; and (iii) obtain mechanistic insights into hydrogen diffusion behavior in Mg-H systems. We do not expect that MD simulations can capture the structural transformation between Mg and MgH₂ due to the short timescale, geometry constraints, and energy barriers from interfacial energy and lattice mismatch. Our strategy is to calculate H diffusivities in Mg and MgH₂ independently. The diffusivities during (de)hydrogenation can then be approximated as volume-fraction-weighted diffusivities of these two phases. We also do not calculate Mg diffusivities since as a host material, Mg is ubiquitous, and its diffusion is not a limiting factor for the reaction kinetics.

II. METHODS AND RESULTS

In conventional nudged elastic band methods [24–26], diffusion energy barriers at 0 K are calculated for distinct atomic jump paths. For Mg-H solid solutions and nonstoichiometric MgH_{*x*} hydrides, the number of possible atomic jump paths with respect to local atomic composition and arrangement is exceedingly large. Even if the barriers for all jump paths could be calculated, implementation of these barriers would require the development of a kinetic Monte Carlo method in order

to predict the apparent overall diffusion performance and the associated overall energy barrier. This problem is straightforwardly addressed by statistically averaged MD simulations [20–23]. In this approach, effective hydrogen diffusivities at finite temperatures can be calculated from the mean-square displacement of hydrogen atoms, which accounts for all atomic jump paths and dynamical correlations. Diffusivities obtained at different temperatures can then be fit to the Arrhenius equation to obtain an overall diffusion energy barrier and an overall preexponential factor. The challenge is that this method is associated with a large statistical error. However, this error can usually be reduced by simply increasing the simulation time [20–23].

Our computational cell for hcp Mg contains 42 (11 $\bar{2}$ 0) planes in the x direction, 12 (0001) planes in the y direction (i.e., y aligns with the c axis), and 24 (1 $\bar{1}$ 00) planes in the z direction. Assuming a tetragonal lattice constant alignment of (a , c , a), our computational cell for the rutile structure of MgH₂ contains 16 (010) planes in the x direction (i.e., x aligns with the c axis), ten (011) planes in the y direction, and 14 (0 $\bar{1}$ 1) planes in the z direction. The Mg crystals measure approximately $65 \times 65 \times 65 \text{\AA}^3$ with 12 096 Mg atoms, and the MgH₂ crystals measure approximately $50 \times 30 \times 45 \text{\AA}^3$ with 2240 Mg atoms and 4480 H atoms. For hcp Mg, we consider four hydrogen compositions: $X_{\text{H}} = 0.0$, 0.00041, 0.01, and 0.1. Here, X_{H} is the atomic fraction of hydrogen with respect to magnesium and $X_{\text{H}} = 0.0$ represents a dilute solution simulated by a single hydrogen atom in the magnesium matrix. These hydrogen atoms are randomly placed in the interstitial sites of the initial configurations. For rutile MgH_{*x*}, we consider two hydrogen compositions: $X_{\text{H}} = 1.7$ and 1.95 (i.e., MgH_{1.7} and MgH_{1.95}). These are achieved by randomly removing 15% and 2.5% of the hydrogen atoms from the stoichiometric MgH₂ lattice.

We apply a previously reported Mg-H bond-order potential (BOP) [27]. This potential reproduces the experimental cohesive energies of the Mg, H₂, and MgH₂ phases. As described above, MD simulations cannot capture the transformation from Mg to MgH₂. However, the previous molecular

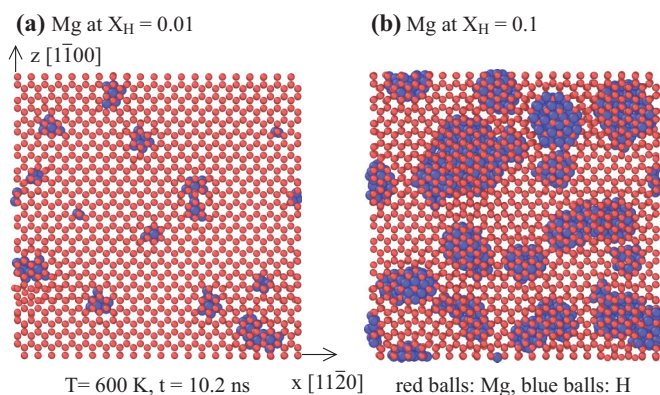


FIG. 1. The xz plane-projected configurations obtained at temperature 600 K and time 10.2 ns for Mg at hydrogen compositions of (a) $X_H = 0.01$ and (b) $X_H = 0.1$.

dynamics simulations [27] have demonstrated that when Mg and H atoms are randomly added to a surface at a stoichiometric ratio of Mg : H = 1 : 2 and a sufficiently high temperature, the adatoms automatically assemble into a structure with the same radial distribution of MgH_2 . Hence, this potential captures the lowest-energy MgH_2 phase. With this potential, we first performed a total of 46 MD simulations with a zero-pressure NPT ensemble (i.e., constant number of atoms, pressure, and temperature) at seven temperatures (400, 450, 500, ..., 700 K) for the four compositions of hcp Mg-H solid solution and nine temperatures (600, 625, 650, ..., 800 K) for the two compositions of rutile MgH_X . A time step size of $dt = 0.5 \text{ fs}$ was used to integrate the atom positions for a total simulation time of 10.2 ns. After discarding the first 0.2 ns for equilibrating the velocity distribution, the hydrogen positions were recorded every $\Delta t = 1.0 \text{ ps}$ for the remaining $t_{\text{MD}} = 10.0 \text{ ns}$ of simulation time. Our previous approach [20–23] was then used to compute diffusivities of hydrogen at different temperatures and compositions.

Before performing Arrhenius analysis of the diffusivity data, we consider effects of temperature and composition on atomic level structures. Figures 1(a) and 1(b) show, respectively, the configurations of Mg at hydrogen compositions of $X_H = 0.01$ and $X_H = 0.1$. In these images the configurations

obtained at a temperature of 600 K and a time of 10.2 ns are projected onto the (0001) basal plane along xz . Figure 1 indicates that for hydrogen composition as low as $X_H = 0.01$, hydrogen atoms segregate to form local Mg-H clusters. The size of the clusters becomes significantly larger for the higher H composition $X_H = 0.1$ than for $X_H = 0.01$. Furthermore, we note that in another simulated case, $X_H = 0.00041$, there are only five H atoms in the entire system. However, even in that case, the H atoms show a tendency to cluster, forming two closely bonded H pairs and one isolated H atom within the Mg matrix after 10.2 ns of annealing. The formation of H pairs suggests that the system has a propensity to form segregated Mg-H clusters under the simulated conditions. In these clusters, the Mg lattice does not change, and H still occupies the interstitial sites. Under the experimental conditions, however, these clusters are likely to transform to MgH_2 hydride. This agrees with the experimental phase diagram [28], which indicates that Mg has an extremely low H solubility.

Analogous images are also provided for MgH_X in Fig. 2. Figures 2(a)–2(c) show the final configurations obtained for $T = 600 \text{ K}$ and $X_H = 1.7$, $T = 800 \text{ K}$ and $X_H = 1.7$, and $T = 800 \text{ K}$ and $X_H = 1.95$, respectively. We can conclude from Figs. 2(a) and 2(b) that for the severely nonstoichiometric $\text{MgH}_{1.7}$ phase, the crystal retains the rutile structure only at low temperatures and becomes distorted at high temperatures. The more stoichiometric $\text{MgH}_{1.95}$ does not exhibit this behavior as the crystal retains the rutile structure up to at least 800 K, as seen in Fig. 2(c). The instability of $\text{MgH}_{1.7}$ is consistent with a significant energetic contribution from the high composition of H vacancies and high vacancy formation energies ($>1 \text{ eV}$ from first-principles calculations [17,29]). The experimental phase diagram [28] is also in agreement with this prediction, as it shows that Mg and H nominally form only the stoichiometric MgH_2 compound.

Arrhenius analysis was applied to the predicted MD diffusivities, and the results are shown in Figs. 3(a) and 3(b) for hydrogen diffusion in Mg and MgH_X respectively. Here “||” and “ \perp ” represent diffusion parallel and normal to the basal plane (the xz plane for Mg and the yz plane for MgH_X). In Fig. 3(a), we omit the $X_H = 0.1$ case because predicted diffusivity is not representative of Mg due to the formation of significant amounts of H-rich clusters, as seen in Fig. 1(b).

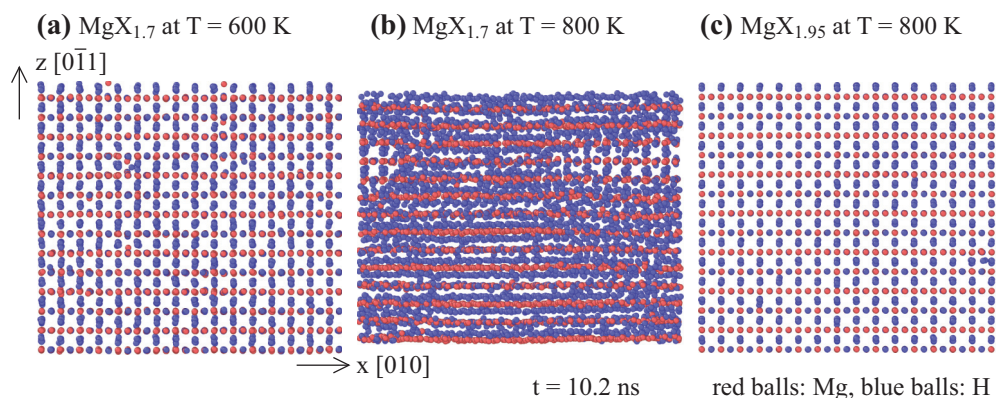
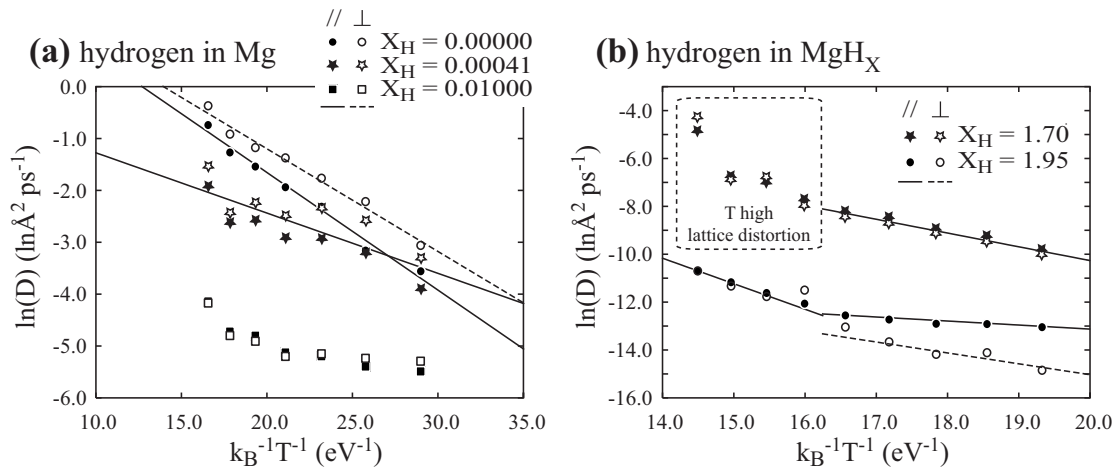


FIG. 2. The xz plane-projected configurations obtained at time 10.2 ns for three MgH_X cases: (a) $T = 600 \text{ K}$, $X_H = 1.7$, (b) $T = 800 \text{ K}$, $X_H = 1.7$, and (c) $T = 800 \text{ K}$, $X_H = 1.95$.

FIG. 3. Hydrogen Arrhenius plots for (a) Mg and (b) MgH_x.

As described above, our goal is to calculate diffusivities in dilute Mg-H solution and MgH₂ only, as we expect that under experimental conditions any nondilute Mg-H solutions will be unstable and should thus rapidly transform to dilute solution + MgH₂. Although final structure obtained for $X_H = 0.01$ also results in H-rich clusters, we include it in Fig. 3(a) for comparison purposes. In Fig. 3(b), we include both low- and high-temperature data regardless of lattice distortions. However, we did not include those temperatures for which lattice distortions are seen in our fitting of the data to analytical expressions, as will be described below.

The results in Fig. 3 reveal several insights. First, diffusivities overall decrease with increasing hydrogen composition for both Mg and MgH_x. Second, the \parallel and \perp diffusivities are similar for MgH_{1.7} but not for Mg and MgH_{1.95}. Third, for Mg, the results at the lowest H composition ($X_H = 0$, effectively infinite dilution of H in Mg) fall better on a single Arrhenius equation than those at higher compositions. For MgH_x at higher hydrogen compositions, different Arrhenius equations appear to be required to describe the low- and high-temperature regimes. This behavior is realistic and has been observed in both experiments [8–12] and simulations [20] of H diffusion in Pd. It occurs as a result of the wide range of diffusion paths having different energy barriers, as will be discussed below. At low temperatures, only low barrier paths are operative. When the temperature increases, diffusion paths with increasingly higher barriers become activated, resulting in an increase of the overall energy barrier.

III. ANALYTICAL EXPRESSIONS

Analytical expressions of diffusivities D as functions of temperature and composition are developed based on the Arrhenius equation:

$$D = D_0 \exp\left(-\frac{Q}{k_B T}\right), \quad (1)$$

where D_0 and Q are, respectively, preexponential factor and activation energy barrier, and k_B and T are, respectively, the Boltzmann constant and temperature. D_0 and Q are assumed

to depend on composition as

$$A(X_H) = A(X_{H,0}) + \frac{A(X_{H,1}) - A(X_{H,0})}{1 + a \exp[-\gamma(X_H - X_{H,0})]}, \quad (2)$$

where A represents D_0 or Q ; $X_{H,0}$ is the stoichiometric composition approximated in our simulations (i.e., $X_{H,0} = 0$ for Mg and $X_{H,0} = 1.95$ for MgH₂), $A(X_{H,0})$ and $A(X_{H,1})$ are the A values at the stoichiometric composition $X_{H,0}$ and another reference composition $X_{H,1}$, respectively; and a and γ are two additional parameters. Note that $X_{H,1}$ is implicit in Eq. (2), but can be thought of as $X_{H,1} \sim 0.0047$ in Mg and $X_{H,1} \sim 1.70$ in MgH_x. With appropriate sign and magnitude of a and γ , Eq. (2) will asymptotically and monotonically change from $A(X_{H,0})$ at $X_{H,0}$ to $A(X_{H,1})$ at $X_{H,1}$. Parameters used in Eq. (2) are fitted to the MD diffusivities, and the fitted parameters are listed in Table II. The lines shown in Fig. 3 are created using these parameters. Clearly, the fitted lines represent the MD data very well.

In Table II, we fit the parameters to different temperature regimes. We emphasize that our analytical expressions pertain to composition ranges of $0.0 \leq X_H \leq 0.00041$ for hcp Mg and $1.7 \leq X_H \leq 2.0$ for rutile MgH_x. Going beyond these composition ranges is not necessary because the Mg-H phase diagram [28] only shows near-perfect stoichiometric Mg and MgH₂ phases. Nevertheless, Eq. (2) is designed to enable D_0 and Q to asymptotically approach their boundary values. Consequently, D_0 and Q will remain near the boundary values even when the value of X_H extends beyond these composition ranges. For instance, Table II shows that the \parallel diffusion barrier in Mg changes from $Q = 0.2264$ eV at $X_H = 0.0$ to near $Q = 0.1149$ eV at $X_H = 0.0047$, but Q will always be bounded to 0.1149 eV by Eq. (2) even if X_H far exceeds 0.0047 . Moreover, our analytical expressions, defined by Eqs. (1) and (2) and the fitted parameters in Table II do not distinguish the \parallel and \perp diffusion for the Mg case at $X_H = 0.00041$, and for the MgH_x cases at $X_H = 1.70$ and at $X_H = 1.95$ and $14 < (k_B T)^{-1} < 16.25$. These choices are consistent with the MD data shown in Fig. 3. Equations (1) and (2), therefore, provide robust diffusivities as functions of temperature and composition for implementation in mesoscale continuum models to simulate (de)hydrogenation kinetics of MgH_x systems.

TABLE II. Parameters used in Eq. (2) for activation energy barrier Q (in eV) and preexponential factor D_0 (in $\text{\AA}^2/\text{ps}$) for different temperature ranges (K).

| Material | Temperature | A | Mode | $A(X_{\text{H},0})$ | $A(X_{\text{H},1})$ | $X_{\text{H},0}$ | a | γ | |
|--|-------------|-------|-------------|---------------------|---------------------|------------------|--------|----------|-------|
| Mg $0.0 \leq X_{\text{H}} \leq 0.00041$ | 400–700 | D_0 | \parallel | 17.6316 | 0.8669 | 0.00 | 10^4 | 38723 | |
| | | | \perp | 15.6831 | | | | | |
| | | Q | \parallel | 0.2264 | 0.1149 | | | | 33672 |
| | | | \perp | 0.1977 | | | | | |
| MgH ₂ $1.7 \leq X_{\text{H}} \leq 2.0$ | 600–714 | D_0 | \parallel | 0.000054264 | 3.3041 | 1.95 | 10^6 | –100 | |
| | | | \perp | 0.0025973 | | | | | |
| | | Q | \parallel | 0.1680 | 0.5729 | | | | |
| | | | \perp | 0.4535 | | | | | |
| | 714–800 | D_0 | \parallel | 109.3774 | 3.3041 | | | | |
| | | | \perp | | | | | | |
| | | Q | \parallel | 1.0618 | 0.5729 | | | | |
| | | | \perp | | | | | | |

According to Table II, our \parallel and \perp hydrogen diffusion energy barriers in Mg are 0.23 and 0.20 eV, respectively, which are in good agreement with the DFT calculations by Ismer *et al.* [15]. Our \parallel and \perp hydrogen diffusion energy barriers in MgH_{1.95} are 0.17 and 0.45 eV, respectively, between 600 and 714 K, and are both equal to 1.06 eV between 714 and 800 K. On the other hand, the hydrogen diffusion barrier in MgH₂ computed with DFT is spread over a wide range: 0.38–0.63 eV from van de Walle and co-workers (Park *et al.* [17]), 0.37–1.12 eV by Sander *et al.* [16], and 0.79–1.1 eV by German and Gebauer [19]. These variations can be attributed in part to differences in assumed defect charge state. As a result, direct comparison with DFT in the case of MgH₂ is challenging. Nevertheless, we attempted to make a head-to-head comparison between empirical potential and our DFT calculations using nudged elastic band methods [24–26] and the same configurations. Details of our DFT methods are described in the Supplemental Material [30] (also see [25,31–33]). For hydrogen diffusion between octahedral and tetrahedral interstitial sites in Mg, we found that the empirical potential gives a barrier of 0.20 eV, matching our DFT value of 0.20 eV. However, for hydrogen vacancy diffusion in MgH_{1.92}, the empirical potential gives an energy barrier of 1.00 eV, whereas DFT gives a barrier of 0.47 eV if we make a neutral vacancy pair defect assumption. Note that this value also differs from that of German and Gebauer [19] where our empirical potential is actually in better agreement, which may be due to the different vacancy identity and the specific choice of jump path. Overall, we conclude that it is not clear what charge should be used for comparison of the DFT simulations with our MD potential, which is instead fitted to the experimental data; nonetheless, our computed diffusion barrier appears to lie within the expected range of available data.

IV. DISCUSSIONS

Molecular statics (MS) energy minimization simulations were performed to gain further insights into the MD results shown in Fig. 3. As mentioned above, the $X_{\text{H}} = 0.00041$ Mg case corresponds to five hydrogen atoms in the simulation volume. Visualization of atomic configurations indicates that

in most cases, these five H atoms reorganize to form two pairs of H dimeric clusters and one isolated H atom within the Mg matrix by the end of the MD simulations. Because dimer diffusion differs from single-atom diffusion, this accounts for the different Arrhenius plots between $X_{\text{H}} = 0.0$ and $X_{\text{H}} = 0.00041$ as shown in Fig. 3(a). To further confirm this, we performed nudged elastic band method [24–26] calculations for several possible jump paths. For a single H atom in Mg, our results indicate that the lowest-energy barriers for \parallel and \perp diffusion are 0.20 and 0.12 eV, respectively. The higher \parallel diffusion barrier than \perp diffusion barrier is consistent with Table II. The 0.20 eV \parallel barrier is close to the corresponding value of 0.2264 eV listed in Table II. The 0.12 eV \perp barrier can also be viewed as supported by the corresponding value of 0.1977 eV listed in Table II because the \perp diffusion cannot proceed consecutively without parallel hops considering that H occupies tetrahedral sites. For H dimer diffusion in Mg, we find it difficult to apply the nudged elastic band method due to the concerted motion of the two atoms. Instead, we performed MD simulations to output configurations every 0.005 ps during both \parallel and \perp jumping events. For each of these configurations, we then performed a separate molecular statics simulation with the coordinate of the primary jump direction of one of the H atoms and all three coordinates of the Mg atoms far away from the hydrogen atoms fixed. From the resulting energies, we obtained energy barriers of 0.109 and 0.190 eV, respectively, for \parallel and \perp diffusion of a H dimer in Mg. Lower-energy barriers for the dimer diffusion compared to single-atom diffusion are consistent with Fig. 3(a) and the 0.1149 eV listed for the dimer diffusion in Table II. Although this phenomenon is somewhat counterintuitive, concerted motion of dimers can be much faster than single-atom diffusion as has been observed both experimentally and theoretically [34,35]. In addition to concerted motion, we can also envision a small barrier when a dimer diffuses through lattice interstices pivoting alternatively on one of its two atoms.

For the higher H compositions, the numerous possible local hydrogen environments require a statistical approach for directly calculating the diffusion barriers. There are 3808 and 4368 H atoms in our MgH_{1.7} and MgH_{1.95} systems. We first performed 3-ns MD simulations in which the temperature was uniformly reduced from 600 to 10 K to anneal the MgH_{1.7}

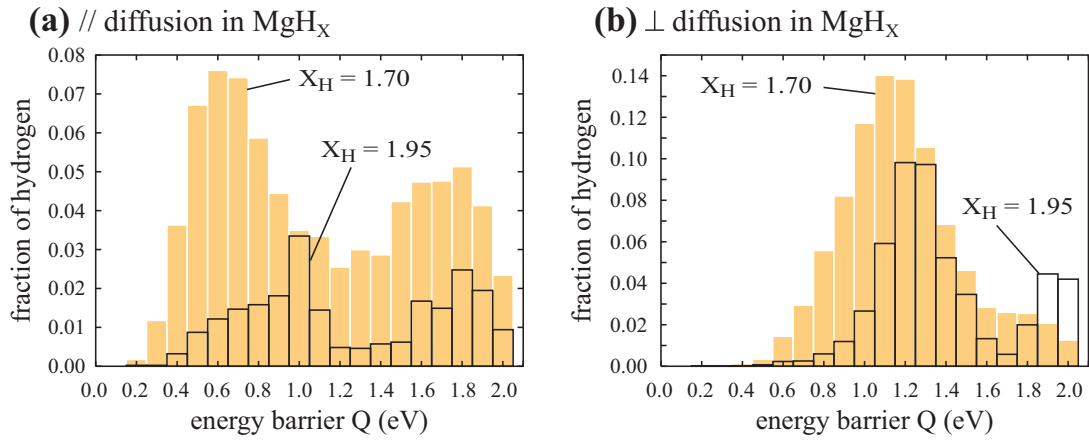


FIG. 4. Hydrogen distribution with respect to energy barriers for (a) \parallel and (b) \perp diffusion within MgH_x .

and $\text{MgH}_{1.95}$ systems. Following our previous approach [22], automated molecular statics simulations were then performed on the final configurations of the MD simulations to calculate diffusion energy barriers for all of the 3808 H atoms in $\text{MgH}_{1.7}$ and all of the 4368 H atoms in $\text{MgH}_{1.95}$. With this approach, six independent simulations are required to determine possible barriers for a H atom moving in each of the six directions $\pm x$, $\pm y$, $\pm z$. In each of these simulations, the H atom is displaced consecutively in small steps in the specified direction, and an energy minimization is performed to relax the system under the constraint that the moving H atom cannot relax in the moving direction but can relax on the plane normal to the moving direction. This way, the molecular statics simulations automatically detect the minimum energy path without knowing the initial and final locations of the jumping atom. Six directions ensure that the minimum energy path has a positive alignment with at least one of the directions. From the relaxed energy profile, the barrier can be identified. In the case where the barriers (either \parallel or \perp diffusion) obtained from the six simulations are not equal, the lowest-energy barrier is always taken as the unique barrier for that H atom. The results are summarized in Figs. 4(a) and 4(b) for \parallel and \perp diffusion, respectively. In Fig. 4, energy barriers are truncated at 2.0 eV and the y axis represents the fraction of H atoms with respect to all H atoms in the system.

The results in Fig. 4 indicate that unlike Mg, MgH_x diffusion energy barriers are distributed over a large energy range. Reducing these ranges to a single barrier observed from MD simulations is not practical. However, Fig. 4 does provide better understanding of the observations in Fig. 3. First, Fig. 4 indicates that energy barriers shift to high values for $\text{MgH}_{1.95}$ as compared to $\text{MgH}_{1.70}$. This is consistent with the MD results in Fig. 3(b) showing that at high temperatures, $\text{MgH}_{1.95}$ has a higher energy barrier than $\text{MgH}_{1.70}$. Figure 4 also shows that fractions of H atoms with low-energy barriers (say, below 1.0 eV) are significantly lower in $\text{MgH}_{1.95}$ than in $\text{MgH}_{1.70}$, consistent with observations in Fig. 3(b) that $\text{MgH}_{1.95}$ has significantly lower diffusivity. Figure 3(b) shows that at low temperatures, the \parallel diffusion has a significantly lower-energy barrier than the \perp diffusion in $\text{MgH}_{1.95}$. This relates to Fig. 4 in which a broad distribution of the $\text{MgH}_{1.95}$ energy barrier

occurs below 0.8 eV for the \parallel diffusion but not for the \perp diffusion. Figure 3(b) also indicates that at high temperatures, the \parallel diffusion and the \perp diffusion in $\text{MgH}_{1.95}$ have a similar energy barrier around 1.1 eV. This is consistent with Fig. 4 in which a similar peak energy barrier can be found for \parallel and \perp diffusion in $\text{MgH}_{1.95}$ (around 1.0 eV or slightly above). We point out that our molecular statics calculations of energy barriers are obtained from a snapshot of MD configuration and our jump paths might also be constrained. Hence, it is unlikely to include all possible jump mechanisms encountered during MD simulations. In this sense, the correlation between MD and MS simulations is satisfactory.

The distributions can also explain the non-Arrhenius behavior for high H compositions in Fig. 3. In a broad distribution, as T increases, the fraction of “accessible” diffusing H atoms in the distribution also increases. Because these newly accessible atoms have a higher barrier, this increases the effective barrier in MD. It is interesting that the distribution in Fig. 4(a) is notably bimodal. In principle, the barrier to hydrogen diffusion is relatively small when there is a nearest-neighbor vacancy. It is expected to increase when there are no nearest-neighbor vacancies, but some second-nearest-neighbor vacancies exist. Whereas actual diffusion processes in MgH_x are more complex, it is not surprising that the barrier distribution exhibits a bimodal feature. This feature suggests simultaneous “faster” and “slower” diffusion channels. However, it is reasonable to assume that as long as a percolating network of “faster” diffusion channels is present, only the lower-energy range of barriers in the first peak of the distribution (<1.2 eV) would be sampled in MD or experiments, at least when the temperature is not too high.

Our simulation results indicate that diffusivities are sensitive to temperature, local composition, and \parallel or \perp measurements. This explains why there is a relatively large scatter for experimentally measured diffusion parameters even when they are measured in the same temperature range. It is thus critical that comparison between simulation results and experimental data be made using the same temperature range, sample composition, and measurement orientation. Simulations must also account for statistics due to the existence of a variety of local jump paths.

V. CONCLUSIONS

Time-averaged MD simulations have been performed to study diffusivities of hydrogen in magnesium and magnesium hydride as a function of both composition and temperature. The following insights into the hydrogen diffusion kinetics in the Mg-H systems have been achieved:

(1) H diffusivities in Mg and MgH₂ are sensitive to H composition. Simulations of (de)hydrogenation kinetics must account for this H composition dependence.

(2) Our MD hydrogen diffusion energy barriers in Mg and MgH_{1.95} are in reasonable agreement with the available experimental values. Moreover, we predict that in both Mg and MgH_x, higher hydrogen compositions show reduced diffusivity.

(3) Although exceptions exist depending on temperatures and compositions, hydrogen diffusivities parallel and normal to the basal planes of Mg and MgH₂ are overall close. For Mg, this can be understood because hydrogen cannot jump consecutively in the normal direction without parallel jumps.

(4) Analytical expressions have been derived to capture well all MD diffusivities obtained at a variety of temperatures and compositions for both Mg and MgH_x, facilitating parametrization of higher-length-scale continuum models.

(5) Insights from molecular-statics-calculated diffusion energy barriers can in general explain the statistically averaged energy barriers obtained from MD simulations, including the non-Arrhenius behavior in magnesium hydride.

ACKNOWLEDGMENTS

Sandia National Laboratories is a multimission laboratory managed and operated by National Technology and Engineering Solutions of Sandia, LLC, a wholly owned subsidiary of Honeywell International, Inc., for the U.S. Department of Energy's National Nuclear Security Administration (NNSA) under Contract No. DE-NA-0003525. Lawrence Livermore National Laboratory is operated for the U.S. Department of Energy under Contract No. DE-AC52-07NA27344. The authors gratefully acknowledge research support from the Hydrogen Materials—Advanced Research Consortium (HyMARC), established as part of the Energy Materials Network under the U.S. Department of Energy, Office of Energy Efficiency and Renewable Energy, Hydrogen and Fuel Cell Technologies Office, under Contracts No. DE-AC04-94AL85000 and No. DE-AC52-07NA27344.

The views and opinions of the authors expressed herein do not necessarily state or reflect those of the U.S. Government or any agency thereof. Neither the U.S. Government nor any agency thereof, nor any of their employees, makes any warranty, expressed or implied, or assumes any legal liability or responsibility for the accuracy, completeness, or usefulness of any information, apparatus, product, or process disclosed, or represents that its use would not infringe privately owned rights.

-
- [1] R. Mohtadi and S. Orimo, The renaissance of hydrides as energy materials, *Nat. Rev. Mater.* **2**, 16091 (2016).
- [2] https://www.energy.gov/sites/prod/files/2017/08/f36/hstt_roadmap_July2017.pdf.
- [3] C. Nishimura, M. Komaki, and M. Amano, Hydrogen permeation through magnesium, *J. Alloys Compd.* **293–295**, 329 (1999).
- [4] J. Renner and H. J. Grabke, Determination of diffusion-coefficients in the hydriding of alloys, *Z. Metallkd.* **69**, 639 (1978).
- [5] J. Cermak and L. Kral, Hydrogen diffusion in Mg-H and Mg-Ni-H alloys, *Acta Mater.* **56**, 2677 (2008).
- [6] X. Yao, Z. H. Zhu, H. M. Cheng, and G. Q. Lu, Hydrogen diffusion and effect of grain size on hydrogenation kinetics in magnesium hydrides, *J. Mater. Res.* **23**, 336 (2008).
- [7] J. F. Fernandez and C. R. Sanchez, Rate determining step in the absorption and desorption of hydrogen by magnesium, *J. Alloys. Compd.* **340**, 189 (2002).
- [8] R. R. Arons, H. G. Bohn, and H. Lutgemier, Investigation of the diffusion of hydrogen in palladium by means of spin-lattice relaxation in the rotating frame, *Solid State Commun.* **14**, 1203 (1974).
- [9] R. R. Arons, Y. Tamminga, and G. de Vries, On the Diffusion of H and D in Pd between 50 and 300 °K, *Phys. Status. Solidi.* **40**, 107 (1970).
- [10] D. A. Cornell and E. F. W. Seymour, Nuclear magnetic resonance study of hydrogen diffusion in palladium and palladium-cerium alloys, *J. Less-Common Met.* **39**, 43 (1975).
- [11] F. M. Mazzolai and H. Zuchner, Hydrogen diffusion in the β -phase of the Pd-H system between 130 and 270 K, *Z. Phys. Chem.* **124**, 59 (1981).
- [12] J. P. Burger, N. J. Poulis, and W. P. A. Hass, Résonance magnétique nucléaire de protons absorbés dans le Pd et des alliages dilués Pd-Fe, *Physica (Amsterdam)* **27**, 514 (1961).
- [13] H. C. Torrey, Effects of translational diffusion on nuclear spin relaxation in simple condensed systems, *Nuovo Cimento* **9**, 95 (1958).
- [14] Y. Nakamori, K. Miwa, A. Ninomiya, H. Li, N. Ohba, S. Towata, A. Züttel, and S. Orimo, Correlation between thermodynamical stabilities of metal borohydrides and cation electronegativities: First-principles calculations and experiments, *Phys. Rev. B* **74**, 045126 (2006).
- [15] L. Ismer, M. S. Park, A. Janotti, and C. G. van de Walle, Interactions between hydrogen impurities and vacancies in Mg and Al: A comparative analysis based on density functional theory, *Phys. Rev. B* **80**, 184110 (2009).
- [16] J. M. Sander, L. Ismer, and C. G. van de Walle, Point-defect kinetics in α - and γ -MgH₂, *Int. J. Hydrogen Energy* **41**, 5688 (2016).
- [17] M. S. Park, A. Janotti, and C. G. van de Walle, Formation and migration of charged native point defects in MgH₂: First-principles calculations, *Phys. Rev. B* **80**, 064102 (2009).

- [18] M. G. Shelyapina, A. V. Vyvodtceva, K. A. Klyukin, O. O. Bavrina, Y. S. Chernyshev, A. F. Privalov, and D. Fruchart, Hydrogen diffusion in metal-hydrogen systems via NMR and DFT, *Int. J. Hydrogen Energy* **40**, 17038 (2015).
- [19] E. German and R. Gebauer, Improvement of hydrogen vacancy diffusion kinetics in MgH₂ by niobium- and zirconium-doping for hydrogen storage applications, *J. Phys. Chem. C* **120**, 4806 (2016).
- [20] X. W. Zhou, T. W. Heo, B. C. Wood, V. Stavila, S. Kang, and M. D. Allendorf, Temperature- and concentration-dependent hydrogen diffusivity in palladium from statistically-averaged molecular dynamics simulations, *Scr. Mater.* **149**, 103 (2018).
- [21] X. W. Zhou, F. El Gabaly, V. Stavila, and M. D. Allendorf, Molecular dynamics simulations of hydrogen diffusion in aluminum, *J. Phys. Chem. C* **120**, 7500 (2016).
- [22] X. W. Zhou, R. Dingreville, and R. A. Karnesky, Molecular dynamics studies of irradiation effects on hydrogen isotope diffusion through nickel crystals and grain boundaries, *Phys. Chem. Chem. Phys.* **20**, 520 (2018).
- [23] X. W. Zhou, R. E. Jones, and J. Gruber, Molecular dynamics simulations of substitutional diffusion, *Comput. Mater. Sci.* **128**, 331 (2017).
- [24] G. Henkelman and H. Jonsson, Improved tangent estimate in the nudged elastic band method for finding minimum energy paths and saddle points, *J. Chem. Phys.* **113**, 9978 (2000).
- [25] G. Henkelman, B. P. Uberuaga, and H. Jonsson, A climbing image nudged elastic band method for finding saddle points and minimum energy paths, *J. Chem. Phys.* **113**, 9901 (2000).
- [26] A. Nakano, A space-time-ensemble parallel nudged elastic band algorithm for molecular kinetics simulation, *Comput. Phys. Commun.* **178**, 280 (2008).
- [27] X. Zhou, S. Kang, T. W. Heo, B. C. Wood, V. Stavila, and M. D. Allendorf, An analytical bond order potential for Mg-H systems, *ChemPhysChem* **20**, 1404 (2019).
- [28] H. Okamoto, H-Mg (hydrogen-magnesium), *J. Phase Equilib.* **22**, 598 (2001).
- [29] S. Hao and D. S. Sholl, Hydrogen diffusion in MgH₂ and NaMgH₃ via concerted motions of charged defects, *Appl. Phys. Lett.* **93**, 251901 (2008).
- [30] See Supplemental Material at <http://link.aps.org/supplemental/10.1103/PhysRevMaterials.4.105401> for density-functional-theory calculations.
- [31] G. Kresse and J. Furthmüller, Efficient iterative schemes for *ab initio* total-energy calculations using a plane-wave basis set, *Phys. Rev. B* **54**, 11169 (1996).
- [32] P. E. Blöchl, Projector augmented-wave method, *Phys. Rev. B* **50**, 17953 (1994).
- [33] J. P. Perdew, K. Burke, and M. Ernzerhof, Generalized Gradient Approximation Made Simple, *Phys. Rev. Lett.* **77**, 3865 (1996).
- [34] A. Emly, E. Kioupakis, and A. van der Ven, Phase stability and transport mechanisms in antiperovskite Li₃OCl and Li₃OBr superionic conductors, *Chem. Mater.* **25**, 4663 (2013).
- [35] R. Kumar, C.-H. Lee, and I.-S. Hwang, Manipulation of single Si adatoms and observation of fast diffusion of Si dimers on a Pb-covered Si(111) surface, *J. Vac. Sci. Technol. A* **35**, 041405 (2017).